

Tunable second-order sideband effects in hybrid optomechanical cavity assisted with a Bose—Einstein condensate

Li-Wei Liu(刘利伟), Chun-Guang Du(杜春光), Guo-Heng Zhang(张国恒), Qiong Chen(陈琼), Yu-Qing Shi(石玉清), Pei-Yu Wang(王培煜), and Yu-Qing Zhang(张玉青)

Citation: Chin. Phys. B, 2022, 31 (**10**): 103701. DOI: 10.1088/1674-1056/ac6ed7

Journal homepage: http://cpb.iphy.ac.cn; http://iopscience.iop.org/cpb

What follows is a list of articles you may be interested in

Nonreciprocal coupling induced entanglement enhancement in a double-cavity optomechanical system

Yuan-Yuan Liu(刘元元), Zhi-Ming Zhang(张智明), Jun-Hao Liu(刘军浩), Jin-Dong Wang(王金东), and Ya-Fei Yu(於亚飞)

Chin. Phys. B, 2022, 31 (**9**): 094203. DOI: 10.1088/1674-1056/ac6499

Manipulation of nonreciprocal unconventional photon blockade in a cavity-driven system composed of an asymmetrical cavity and two atoms with weak dipole-dipole interaction

Xinqin Zhang(张新琴), Xiuwen Xia(夏秀文), Jingping Xu(许静平), Haozhen Li(李浩珍), Zeyun Fu(傅泽云), and Yaping Yang(羊亚平)

Chin. Phys. B, 2022, 31 (**7**): 074204. DOI: 10.1088/1674-1056/ac523f

Measuring gravitational effect of superintense laser by spin-squeezed Bose—Einstein condensates interferometer

Eng Boon Ng and C. H. Raymond Ooi

Chin. Phys. B, 2022, 31 (**5**): 053701. DOI: 10.1088/1674-1056/ac4231

Influence of driving ways on measurement of relative phase in a two-atoms cavity system

Daqiang Bao(包大强), Jingping Xu(许静平), Yaping Yang(羊亚平)

Chin. Phys. B, 2020, 29 (**4**): 043702. DOI: 10.1088/1674-1056/ab7904

Controllable optical bistability of Bose–Einstein condensate in an optical cavity with Kerr medium

Zheng Qiang, Li Sheng-Chang, Zhang Xiao-Ping, You Tai-Jie, Fu Li-Bin

Chin. Phys. B, 2012, 21 (**9**): 093702. DOI: 10.1088/1674-1056/21/9/093702

Tunable second-order sideband effects in hybrid optomechanical cavity assisted with a Bose–Einstein condensate

Li-Wei Liu(刘利伟)[1,2], Chun-Guang Du(杜春光)[3,†], Guo-Heng Zhang(张国恒)[1], Qiong Chen(陈琼)[1], Yu-Qing Shi(石玉清)[1], Pei-Yu Wang(王培煜)[1], and Yu-Qing Zhang(张玉青)[4]

[1] *College of Electrical Engineering, Northwest Minzu University, Lanzhou* 730000, *China*
[2] *Visiting Scholar, Department of Physics, Tsinghua University, Beijing* 100084, *China*
[3] *State Key Laboratory of Low-Dimensional Quantum Physics and Department of Physics, Tsinghua University, Beijing* 100084, *China*
[4] *School of Physics and Electronics Science, Hunan University of Science and Technology, Xiangtan* 411201, *China*

(Received 28 January 2022; revised manuscript received 29 April 2022; accepted manuscript online 12 May 2022)

We theoretically investigated a second-order optomechanical-induced transparency (OMIT) process of a hybrid optomechanical system (COMS), which a Bose–Einstein condensate (BEC) in the presence of atom–atom interaction trapped inside a cavity with a moving end mirror. The advantage of this hybrid COMS over a bare COMS is that the frequency of the second mode is controlled by the s-wave scattering interaction. Based on the traditional linearization approximation, we derive analytical solutions for the output transmission intensity of the probe field and the dimensionless amplitude of the second-order sideband (SS). The numerical results show that the transmission intensity of the probe field and the dimensionless amplitude of the SS can be controlled by the s-wave scattering frequency. Furthermore, the control field intensities, the effective detuning, the effective coupling strength of the cavity field with the Bogoliubov mode are used to control the transmission intensity of the probe field and the dimensionless amplitude of the SS.

Keywords: second-order sideband, Bose–Einstein condensate, cavity optomechanical

PACS: 37.30.+i, 42.50.Pq, 42.50.Wk **DOI:** 10.1088/1674-1056/ac6ed7

1. Introduction

Cavity optomechanical system (COMS) describes the interaction between the radiation pressure and mechanical degrees of freedom, which has been developing rapidly in recent years.[1–3] These COMS can induce exciting phenomena, such as optomechanical-induced transparency (OMIT),[4–7] slow and fast light,[8,9] optical bistability,[10–13] higher-order sidebands (HS),[14–19] sideband comb,[20–23] optomechanical chaos,[24–26] quantum entanglement,[27,28] and so on. Some phenomena can be explained by the linearized optomechanical interactions, while the others need to be explained by the nonlinear interactions. In recent years, the second-order sideband (SS) or even HS effect induced by the nonlinear optomechanical interactions have attracted much attention. However, SS and HS effects are generally much weaker than the detected signal, it is difficult to detect or exploit in COMS. Therefore, generating and amplifying the SS and HS become an essential task in many physical fields, including precision measurement of DNA molecules properties,[29] precise sensing of charges[30–32] and mass,[33] weak force and single particle detection,[34,35] excellent optical frequency combs,[36–39] and so on.

There are many COMS that share the same properties, such as Fabry–Pérot cavity with moving end mirror or a membrane in the middle,[40–47] and a Bose–Einstein condensate (BEC) trapped inside an optical cavity.[48–53] Great progress has been made in the study of various characteristics of a hybrid COMS composed of BEC, such as quantum entanglement generation,[54–57] quantum ground-state cooling,[58–61] coherent quantum noise cancelation,[62,63] Fano resonances and OMIT with single and multiple windows,[64–66] quantum router,[67] and so on.

In this paper, we study the tunable SS effects in a hybrid COMS, where a cigar-shaped BEC is trapped inside an optical cavity with a moving end-mirror.[68] In our model, the laser field in the cavity has two functions: it excites the momentum side mode of the BEC, and the cavity mode will act as a spring between ultra-cold atoms of BEC and mechanical resonator and couples the motion of both.[6] In Section 2, we give the Hamiltonian of the hybrid COMS consisting of a BEC with s-wave scattering interaction trapped inside a cavity with a moving end mirror under the condition of discrete mode approximation. We derive the analytic expression of the transmission intensity $|t_{\rm p}|^2$ of the probe field and the dimensionless amplitude $\eta_{\rm s}$ of the SS by the quantum-Langevin equations. Because of the atom–atom interaction, the interaction between atoms–cavity can be enhanced by the atoms collectively couple to the same optical cavity.[49,50] Moreover, the frequency of the Bogoliubov mode depends on the s-wave scattering frequency $\omega_{\rm sm}$ of the atomic collision, we can obtain the controllability of the frequency of the Bogoliubov mode by the s-wave scattering interaction.[69,70] The numerical results show

†Corresponding author. E-mail: ducg@mail.tsinghua.edu.cn
© 2022 Chinese Physical Society and IOP Publishing Ltd

that the effect of the transmission intensity and the dimensionless amplitude of the SS can be controlled effectively by the control field intensities, the nonlinear atom–atom interaction, the effective detuning, the effective coupling strength of the optical field with the Bogoliubov mode in Section 3. Finally, our summary is given in Section 4.

2. System and method

The hybrid COMS we considered is shown schematically in Fig. 1, consisting of a cigar-shaped BEC of N two-level atoms with mass $m_{\rm a}$ and transition frequency $\omega_{\rm a}$ inside a single-mode, high-finesse Fabry–Pérot cavity with length L whose end mirror is free oscillated with frequency $\omega_{\rm m}$. The cavity field is driven by a strong pump laser field with frequency $\omega_{\rm pu}$ accompanying a weak probe laser field with frequency $\omega_{\rm pr}$ through one of its mirror. We assume the BEC to be confined in a cylindrically symmetric trap with a transverse trapping frequency $\omega_{\perp}$ and negligible longitudinal confinement along the x direction. Then we can describe the dynamics within an effective one-dimensional model by quantizing the atomic motional degree of freedom along the x axis only. Furthermore, the laser pump is far detuned from the atomic resonance, *i.e.*, $\Delta_{\rm a}=\omega_{\rm pu}-\omega_{\rm a}\gg\gamma_{\rm a}$, here $\gamma_{\rm a}$ is the atomic linewidth, then the excited electronic state of the atoms can be adiabatically eliminated and spontaneous emission can be neglected, so the atomic wave function can be described by the scalar quantum field $\Psi(x)$.[60] The Hamiltonian can be written as

$$\begin{aligned}\hat{H} =& \int_0^L {\rm d}x\Psi^{\dagger}(x)\left[\frac{-\hbar^2}{2m_{\rm a}}\frac{{\rm d}^2}{{\rm d}x^2}+\hbar U_0\cos^2(kx)\hat{c}^{\dagger}\hat{c}\right.\\ &\left.+\frac{1}{2}U_{\rm s}\Psi^{\dagger}(x)\Psi(x)\right]\Psi(x)\\ &+\hbar\omega_{\rm c}\hat{c}^{\dagger}\hat{c}-{\rm i}\hbar E_{\rm pu}\left(\hat{c}\,{\rm e}^{{\rm i}\omega_{\rm pu}t}-\hat{c}^{\dagger}\,{\rm e}^{-{\rm i}\omega_{\rm pu}t}\right)\\ &-{\rm i}\hbar E_{\rm pr}\left(\hat{c}\,{\rm e}^{{\rm i}\omega_{\rm pr}t}-\hat{c}^{\dagger}\,{\rm e}^{-{\rm i}\omega_{\rm pr}t}\right)\\ &+\frac{\hbar\omega_{\rm m}}{2}\left(\hat{p}^2+\hat{q}^2\right)-\hbar G\hat{c}^{\dagger}\hat{c}\hat{q}. \end{aligned}\tag{1}$$

Here $\hat{c}$ is the cavity field's annihilation operator and central frequency $\omega_{\rm c}=n\pi c/L$, $U_0=g_0^2/\Delta_{\rm a}$ is the maximum light shift which an atom experiences in the cavity mode, $\Delta_{\rm a}$ is the atomic-pump detuning, and g_0 is the maximum coupling strength that between a single atom and a single intracavity photon. $U_{\rm s}=(4\pi\hbar^2a_{\rm s}/m_{\rm a})$ and $a_{\rm s}$ is the two body s-wave scattering length. The second and third terms in the second line of Eq. (1) describe the energy of the strong pump laser field and the weak probe laser field, $E_{\rm pu}$ and $E_{\rm pr}$ are amplitudes of the two lasers with $|E_{\rm pu}|=\sqrt{2P_{\rm pu}\kappa/\hbar\omega_{\rm pu}}$ and $|E_{\rm pr}|=\sqrt{2P_{\rm pr}\kappa/\hbar\omega_{\rm pr}}$, where $p_{\rm pu}$ and $p_{\rm pr}$ are powers of the pump laser and the probe laser, respectively, and κ is the decay rate of the intra-cavity optical mode. The last line of Eq. (1) describes the Hamiltonian of the moving mirror and the mirror–cavity interaction, $\hat{q}$ ($\hat{p}$) are the position (momentum) operator of the moving mirror, and the coupling strength (that between mirror–cavity coupling) is $G=(\omega_{\rm c}/L)\sqrt{\hbar/m\omega_{\rm m}}$.

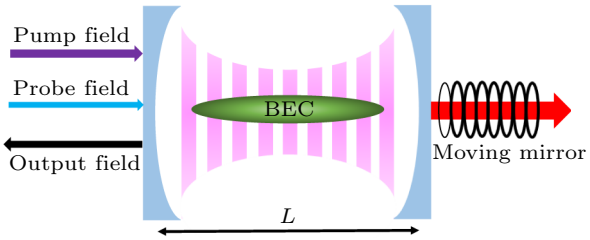


Fig. 1. The hybrid optomechanical system consisting of a BEC trapped inside an optical cavity with a moving end-mirror. The cavity is driven by a strong pump laser with frequency $\omega_{\rm pu}$ and a weak probe laser with frequency $\omega_{\rm pr}$.

In the following, we will use the discrete mode approximation for the expansion of the matter–wave function $\Psi(x)$. Firstly, because of the interaction of the matter field with the optical field, the atoms are excited from the ground state of the condensate into states with momenta $p=\pm2\hbar k,\pm4\hbar k,\ldots$ which means that each of them may form a number of quasi-momenta, where k is the wave vector of the cavity photons. Furthermore, in the simplest case, it is considered that the weakly interacting regime, $U_0\langle\hat{c}^{\dagger}\hat{c}\rangle\leq10\omega_{\rm r}$ ($\omega_{\rm r}=\hbar k^2/2m_{\rm a}$ is the recoil frequency of the condensate atoms). Then only the first two symmetric momentum side modes with moment $\pm2\hbar k$ were excited by fluctuations as a result of the atom–light interaction. Considering the parity conservation and the Bogoliubov approximation, the atomic field operator can be expanded as follows:[50]

$$\Psi(x)=\sqrt{\frac{1}{L}}\hat{a}_0+\sqrt{\frac{2}{L}}\cos(2kx)\hat{a}_2.\tag{2}$$

Here $\hat{a}_0$ and $\hat{a}_2$ are bosonic annihilation operators for atoms in the zero-momentum state and side-mode components, respectively. The total number of atoms is $\hat{a}_0^{\dagger}\hat{a}_0+\hat{a}_2^{\dagger}\hat{a}_2=N$. Because the population in the zero-momentum state is much larger than the population in the side-mode state, we can neglect the population in the side-mode state. We use $\hat{a}_0^{\dagger}\hat{a}_0\simeq N$, and $\hat{a}$ instead of $\hat{a}_2$. The Hamiltonian of the hybrid COMS can be expressed as follows:[68]

$$\begin{aligned}\hat{H} =& \hbar\omega_{\rm m}'\hat{a}^{\dagger}\hat{a}+\frac{1}{4}\hbar\omega_{\rm sm}(\hat{a}^2+\hat{a}^{\dagger2})+\hbar g(\hat{a}^{\dagger}+\hat{a})\hat{c}^{\dagger}\hat{c}\\ &+\hbar\omega_{\rm c}'\hat{c}^{\dagger}\hat{c}+\frac{\hbar\omega_{\rm m}}{2}\left(\hat{p}^2+\hat{q}^2\right)-\hbar G\hat{c}^{\dagger}\hat{c}\hat{q}\\ &-{\rm i}\hbar E_{\rm pu}\left(\hat{c}\,{\rm e}^{{\rm i}\omega_{\rm pu}t}-\hat{c}^{\dagger}\,{\rm e}^{-{\rm i}\omega_{\rm pu}t}\right)\\ &-{\rm i}\hbar E_{\rm pr}\left(\hat{c}\,{\rm e}^{{\rm i}\omega_{\rm pr}t}-\hat{c}^{\dagger}\,{\rm e}^{-{\rm i}\omega_{\rm pr}t}\right).\end{aligned}\tag{3}$$

Here $\omega_{\rm m}'$ is the frequency of the Bogoliubov mode, where $\omega_{\rm m}'=4\omega_{\rm r}+\omega_{\rm sm}=4\frac{\hbar k^2}{2m}+\omega_{\rm sm}$, $\omega_{\rm sm}=\frac{8\pi\hbar a_{\rm s}N}{m_{\rm a}L\omega^2}$ is the s-wave scattering frequency, and the coupling strength (that between

the Bogoliubov-optical mode) is $g = (U_0/2)\sqrt{N/2}$. $\omega_c' = \omega_c + (1/2)U_0N$, $(1/2)U_0N$ is the frequency shift of the empty cavity resonance induced by the Bogoliubov mode.

Defining the Bogoliubov mode quadratures $\hat{Q} = (\hat{a} + \hat{a}^\dagger)/\sqrt{2}$ and $\hat{P} = (\hat{a} - \hat{a}^\dagger)/\sqrt{2}\mathrm{i}$, we can obtain the following Hamiltonian:

$$\frac{\hbar\omega_m'^+}{2}(\hat{P}^2) + \frac{\hbar\omega_m'^-}{2}(\hat{Q}^2) - \hbar G\hat{c}^\dagger\hat{c}\hat{Q},$$

here $\omega_m'^\pm = \omega_m' \pm (1/2)\omega_{sm}$. Next, we redefine the expressions of the Bogoliubov mode quadratures as $\hat{X} = \chi\hat{Q}$ and $\hat{Y} = (1/\chi)\hat{P}$, where $\chi = (\omega_m'^+/\omega_m'^-)^{1/4}$. In the following, we can rewrite Eq. (3) in a frame rotating with the frequency ω_{pu}:[60]

$$\hat{H} = \hbar\Omega_c(\hat{X}^2 + \hat{Y}^2) + \hbar\xi\hat{X}\hat{c}^\dagger\hat{c} + \frac{\hbar\omega_m}{2}(\hat{p}^2 + \hat{q}^2) - \hbar G\hat{c}^\dagger\hat{c}\hat{q} + \hbar\Delta_c\hat{c}^\dagger\hat{c} - \mathrm{i}\hbar E_{pu}(\hat{c} - \hat{c}^\dagger) - \mathrm{i}\hbar E_{pr}\left(\hat{c}\,\mathrm{e}^{\mathrm{i}\delta t} - \hat{c}^\dagger\,\mathrm{e}^{-\mathrm{i}\delta t}\right). \quad (4)$$

Here $\Omega_c = \sqrt{\omega_m'^+\omega_m'^-}$ is the frequency of the Bogoliubov mode of the BEC, $\xi = (1/\chi)g$ is the coupling strength. $\Delta_c = \omega_c' - \omega_{pu}$, Δ_c is the effective Stark-shift detuning, and $\delta = \omega_{pr} - \omega_{pu}$ is the probe–pump detuning. The Hamiltonian in Eq. (4) corresponds to a three-mode COMS, the first is atomic Bogoliubov mode $(\hat{X}, \hat{Y})$ and the second is mechanical mode $(\hat{p}, \hat{q})$ interacting with the cavity simultaneously. The influence of atom–atom interaction in this Hamiltonian is reflected in the frequency of the Bogoliubov mode Ω_c and the coupling strength ξ.

In this paper, we focus on the average response of the COMS to the probe field, so that all operators ($\hat{c}$, $\hat{X}$, $\hat{Y}$, $\hat{p}$, and $\hat{q}$) can be reduced to expected values. According to the commutation relation $[\hat{a}, \hat{a}^\dagger] = 1$, $[\hat{X}, \hat{Y}] = \mathrm{i}$, and $[\hat{p}, \hat{q}] = \mathrm{i}$, adding the damping terms, the equations can be expressed as

$$\frac{\mathrm{d}\langle c\rangle}{\mathrm{d}t} = -(\mathrm{i}\Delta_c + \kappa + \mathrm{i}\xi\langle X\rangle - \mathrm{i}G\langle q\rangle)\langle c\rangle + E_{pu} + E_{pr}\,\mathrm{e}^{-\mathrm{i}\delta t}, \quad (5)$$

$$\frac{\mathrm{d}\langle X\rangle}{\mathrm{d}t} = \Omega_c\langle Y\rangle - \gamma_c\langle X\rangle, \quad (6)$$

$$\frac{\mathrm{d}\langle Y\rangle}{\mathrm{d}t} = -\Omega_c\langle X\rangle - \xi\langle c^\dagger\rangle\langle c\rangle - \gamma_c\langle Y\rangle, \quad (7)$$

$$\frac{\mathrm{d}\langle q\rangle}{\mathrm{d}t} = \omega_m\langle p\rangle, \quad (8)$$

$$\frac{\mathrm{d}\langle p\rangle}{\mathrm{d}t} = -\omega_m\langle q\rangle + G\langle c^\dagger\rangle\langle c\rangle - \gamma_m\langle p\rangle, \quad (9)$$

where γ_c and γ_m are the decay rates of atoms and the mechanical resonator, respectively. For simplicity, using the mean field assumption $\langle c^\dagger c\rangle = \langle c^\dagger\rangle\langle c\rangle$, $\langle Xc\rangle = \langle X\rangle\langle c\rangle$, and $\langle Qc\rangle = \langle Q\rangle\langle c\rangle$, and ignoring some small quantum correlations but without loss of generality. In the weak laser driving regime, especially in the strong coupling region of a single photon, the nonlinear interaction between the cavity field and atomic Bogoliubov mode and the mechanical mode affect the response of the system to the probe field. Next, using the perturbation method to deal with Eqs. (5)–(9). The total solution of cavity and atomic Bogoliubov mode and the mechanical mode can be written as $\langle c\rangle = c_0 + \delta c$, $\langle X\rangle = X_0 + \delta X$, and $\langle q\rangle = q_0 + \delta q$. The steady-state solution of Eqs. (5)–(9) can be obtained as

$$c_0 = \frac{E_{pu}}{\sqrt{\kappa^2 + \Delta^2}}, \quad (10)$$

$$X_0 = -\frac{\xi\Omega_c|c_0|^2}{\Omega_c^2 + \gamma_c^2}, \quad (11)$$

$$q_0 = \frac{G|c_0|^2}{\omega_m}, \quad (12)$$

where $\Delta = \Delta_c + \xi X_0 - Gq_0$ is the effective detuning, c_0 is the steady state amplitude of the cavity field, X_0 and q_0 are the new equilibrium position of the collective oscillation of the BEC and mechannical displacement for the static solution, respectively. Next, we consider the perturbation made by the probe field and ignore the high-order terms, the equations for the fluctuations can be obtained as

$$\frac{\mathrm{d}\delta c}{\mathrm{d}t} = -(\mathrm{i}\Delta + \kappa)\delta c - \mathrm{i}\xi(c_0\delta X + \delta c\delta X) + \mathrm{i}G(c_0\delta q + \delta c\delta q) + E_{pr}\,\mathrm{e}^{-\mathrm{i}\delta t}, \quad (13)$$

$$\frac{\mathrm{d}\delta X}{\mathrm{d}t} = \Omega_c\delta Y - \gamma_c\delta X, \quad (14)$$

$$\frac{\mathrm{d}\delta Y}{\mathrm{d}t} = -\Omega_c\delta X - \xi(c_0^*\delta c + c_0\delta c^* + \delta c\delta c^*) - \gamma_c\delta Y, \quad (15)$$

$$\frac{\mathrm{d}\delta q}{\mathrm{d}t} = \omega_m\delta p, \quad (16)$$

$$\frac{\mathrm{d}\delta p}{\mathrm{d}t} = -\omega_m\delta q + G(c_0^*\delta c + c_0\delta c^* + \delta c\delta c^*) - \gamma_m\delta p. \quad (17)$$

Under the second-order sideband approximation, the solutions of Eqs. (13)–(17) can be written as[14–19]

$$\delta c = c_1^-\,\mathrm{e}^{-\mathrm{i}\delta t} + c_1^+\,\mathrm{e}^{\mathrm{i}\delta t} + c_2^-\,\mathrm{e}^{-2\mathrm{i}\delta t} + c_2^+\,\mathrm{e}^{2\mathrm{i}\delta t}, \quad (18)$$

$$\delta X = X_1^-\,\mathrm{e}^{-\mathrm{i}\delta t} + X_1^+\,\mathrm{e}^{\mathrm{i}\delta t} + X_2^-\,\mathrm{e}^{-2\mathrm{i}\delta t} + X_2^+\,\mathrm{e}^{2\mathrm{i}\delta t}, \quad (19)$$

$$\delta Y = Y_1^-\,\mathrm{e}^{-\mathrm{i}\delta t} + Y_1^+\,\mathrm{e}^{\mathrm{i}\delta t} + Y_2^-\,\mathrm{e}^{-2\mathrm{i}\delta t} + Y_2^+\,\mathrm{e}^{2\mathrm{i}\delta t}, \quad (20)$$

$$\delta q = q_1^-\,\mathrm{e}^{-\mathrm{i}\delta t} + q_1^+\,\mathrm{e}^{\mathrm{i}\delta t} + q_2^-\,\mathrm{e}^{-2\mathrm{i}\delta t} + q_2^+\,\mathrm{e}^{2\mathrm{i}\delta t}, \quad (21)$$

$$\delta p = p_1^-\,\mathrm{e}^{-\mathrm{i}\delta t} + p_1^+\,\mathrm{e}^{\mathrm{i}\delta t} + p_2^-\,\mathrm{e}^{-2\mathrm{i}\delta t} + p_2^+\,\mathrm{e}^{2\mathrm{i}\delta t}. \quad (22)$$

The physical picture of Eq. (18) is that when the control field and the probe field incident into the cavity, due to the nonlinear interaction terms $\delta c\delta X$, $\delta c\delta q$, and $\delta c\delta c^*$, a series of frequencies output fields $\omega_{pr} \pm n\delta$ are generated, where n is an integer representing the sideband order. In Eq. (18) the parameters c_1^- and c_1^+ are the coefficients of the first upper sideband (the anti-Stokes field with frequency $\omega_{pr} + \delta$) and lower sideband (the Stokes field with frequency $\omega_{pr} - \delta$). Similarly, c_2^- and c_2^+ in Eq. (18) are the coefficients of the second upper (with frequency $\omega_{pr} + 2\delta$) and lower sidebands (with frequency $\omega_{pr} - 2\delta$). It is well known that the coefficient

of the SS is much smaller than that of the first-order sideband. We only consider first-order and SS and ignore the HS effect.[14–19]

And then we use the following input–output relation:

$$c_{\rm out}(t) = c_{\rm in}(t) - \sqrt{2\kappa}c(t), \tag{23}$$

where $c_{\rm in}$ is the input operator and $c_{\rm out}$ is the output operator. For our hybrid COMS, we obtain the output field in the original frame

$$\begin{aligned} c_{\rm out}(t) \;=\; & \left(E_{\rm pu}/\sqrt{2}\kappa - \sqrt{2}\kappa c_0\right) {\rm e}^{-{\rm i}\omega_{\rm pu}t} \\ & + \left(E_{\rm pr}/\sqrt{2}\kappa - \sqrt{2}\kappa c_1^-\right) {\rm e}^{-{\rm i}(\omega_{\rm pu}+\delta)t} \\ & - \sqrt{2}\kappa c_1^+ {\rm e}^{-{\rm i}(\omega_{\rm pu}-\delta)t} - \sqrt{2}\kappa c_2^- {\rm e}^{-{\rm i}(\omega_{\rm pu}+2\delta)t} \\ & - \sqrt{2}\kappa c_2^+ {\rm e}^{-{\rm i}(\omega_{\rm pu}-2\delta)t}. \end{aligned} \tag{24}$$

The terms $(E_{\rm pu}/\sqrt{2}\kappa - \sqrt{2}\kappa c_0){\rm e}^{-{\rm i}\omega_{\rm pu}t}$ and $(E_{\rm pr}/\sqrt{2}\kappa - \sqrt{2}\kappa c_1^-){\rm e}^{-{\rm i}(\omega_{\rm pu}+\delta)t}$ describe the output fields with the frequencies of the driven field $\omega_{\rm pu}$ and the probe field $\omega_{\rm pr}$. The term $\sqrt{2}\kappa c_1^+ {\rm e}^{-{\rm i}(\omega_{\rm pu}-\delta)t}$ is the Stokes process at the frequency $2\omega_{\rm pu} - \omega_{\rm pr}$ in Eq. (24). The transmission of the probe field is defined as

$$t_{\rm p} = \frac{E_{\rm pr}/\sqrt{2}\kappa - \sqrt{2}\kappa c_1^-}{E_{\rm pr}/\sqrt{2}\kappa}, \tag{25}$$

where the c_1^- can be obtained from Eq. (A11) (for details see Appendix A).

The terms of

$$-\sqrt{2}\kappa c_2^- {\rm e}^{-{\rm i}(\omega_{\rm pu}+2\delta)t} \quad \text{and} \quad -\sqrt{2}\kappa c_2^+ {\rm e}^{-{\rm i}(\omega_{\rm pu}-2\delta)t}$$

individually describe the sideband process of second-order upper (with frequency $2\omega_{\rm pr} - \omega_{\rm pu}$) and lower (with frequency $3\omega_{\rm pu} - \omega_{\rm pr}$) sidebands. In the following, we define the dimensionless amplitude of the SS as

$$\eta_{\rm s} = \left| \frac{c_2^-}{E_{\rm pr}/\sqrt{2}\kappa} \right|, \tag{26}$$

where the c_2^- can be obtained from Eq. (A28) (for details see Appendix A).

3. Results and discussion

In order to explicitly illustrate the properties of the transmission intensity of the probe field and the dimensionless amplitudes of the SS in the hybrid COMS, the realistic parameters of our system are selected as follows.[49,50] Considering $N = 2.3 \times 10^4$ ^{87}Rb atoms inside a single-mode cavity with length $L = 1.78 \times 10^{-4}$ m, which is driven by the external field with wavelength $\lambda_{\rm p} = 780$ nm and with decay rate $\kappa = 2\pi \times 1.3$ kHz. Further, the recoil of atomic mode is $\omega_{\rm r} = 2\pi \times 3.8$ kHz with damping rate $\gamma_{\rm c} = 0.001\kappa$. The moving end mirror with frequency $\omega_{\rm m} = 1.1\Omega_{\rm c}$ and damping rate $\gamma_{\rm m} = 0.001\kappa$. We are based on the following two conditions: one is known as the resolved sideband condition $\omega_{\rm m} \gg \kappa$, to ensure that we can distinguish the normal mode splitting. The second one is that the cavity is driven by the red-detuned cavity field $\Delta = (\omega_{\rm m} + \Omega_{\rm c})/2 = \bar{\omega}$.

Physically, when the coupling field $\omega_{\rm c}$ is red detuned by an amount $\bar{\omega}$ and $\omega_{\rm pr}$ approach the cavity frequency in the three-mode COMS, the level scheme of the standard COMS is similar to that of a three-level medium as shown in Fig. 2. The $|1\rangle \leftrightarrow |3\rangle$ transition is the excitation at the weak probe laser, and the strong pump laser is red detuned by an amount $\bar{\omega} = (\omega_{\rm m} + \Omega_{\rm c})/2$ to induce OMIT. Due to radiation pressure, additional coherence is created between the mechanical modes, resulting in OMIT splitting. From Fig. 2, the destructive interference has two paths when the two resonant frequencies are different, which means that the probe field has two OMIT Windows. Because of the radiation pressure, OMIT is analogous to driving hyperfine transitions in a Λ-type three-level atomic system via a radio-frequency or microwave field.[42]

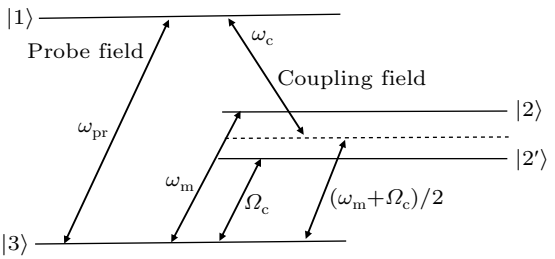


Fig. 2. The level diagram of the optomechanical system. The $|1\rangle \leftrightarrow |3\rangle$ transition is the excitation at the cavity frequency, the coupling laser is red detuned by an amount $\bar{\omega} = (\omega_{\rm m} + \Omega_{\rm c})/2$ to induce OMIT.

Next, we focus on the features of the transmission intensity and the dimensionless amplitude of the SS in this hybrid COMS based on the analytical expressions in Eqs. (25) and (26). In order to modulate the hybrid COMS, we will study the dependence of the transmission intensity and the dimensionless amplitude of the SS on the COMS parameters, including the control field intensity, the nonlinear atom–atom interaction, the effective detuning, the effective coupling strength of the cavity field with the Bogoliubov mode.

Firstly, the transmission intensity $|t_{\rm p}|^2$ of the probe field and the dimensionless amplitude $\eta_{\rm s}$ of the SS are plotted as a function of the probe–pump detuning $\delta/\bar{\omega}$ for different the control field intensities: (i) $E_{\rm pu} = 0.075\omega_{\rm m}$, (ii) $E_{\rm pu} = 0.1\omega_{\rm m}$, (iii) $E_{\rm pu} = 0.4\omega_{\rm m}$ in Fig. 3. As clearly seen from Figs. 3(a) and 3(d), figure 3(a) shows that there is only one transparent window at the $\omega = \bar{\omega} - \omega_0$, that means the probe field is almost completely absorbed in another transparent window

at $\omega = \bar{\omega} + \omega_0$. From Fig. 3(d), the dimensionless amplitude of the SS exhibits two normal dips at $\omega = \bar{\omega} + \omega_0$ and $\omega = \bar{\omega} - \omega_0$, here ω_0 is the small deviation from the central frequency $\bar{\omega}$. Figures 3(b) and 3(e) show the dimensionless transmission intensity $|t_p|^2$ and the dimensionless amplitude η_s of the SS vary with $\delta/\bar{\omega}$ under a stronger control field $E_{pu} = 0.1\omega_m$. Figure 3(b) shows that there are two transparent windows at $\omega = \bar{\omega} \pm \omega_0$, which, however, are not very deep. Figure 3(e) shows the dimensionless amplitude η_s of the SS under the same control field, one can see that η_s also becomes obvious near exhibit two normal dips at the $\omega = \bar{\omega} \pm \omega_0$. Figures 3(c) and 3(f) show the transmission intensity $|t_p|^2$ and the dimensionless amplitude η_s of the SS vary with $\delta/\bar{\omega}$ under much stronger control field $E_{pu} = 0.4\omega_m$. On the one hand, the transmission intensity $|t_p|^2$ and the dimensionless amplitude η_s of the SS exhibit two normal dips at the $\omega = \bar{\omega} \pm \omega_0$. On the other hand, one obvious phenomenon is that the SS also shows two windows, and the windows become more and more obvious with the increase of the intensity of the control field. The physical effects can be explained by the radiation pressure coupling of cavity modes. OMIT relies on quantum interference, the coupling between the cavity field and the Bogoliubov mode and the mirror breaks the symmetry of the OMIT interference, then a single OMIT window is split into two.

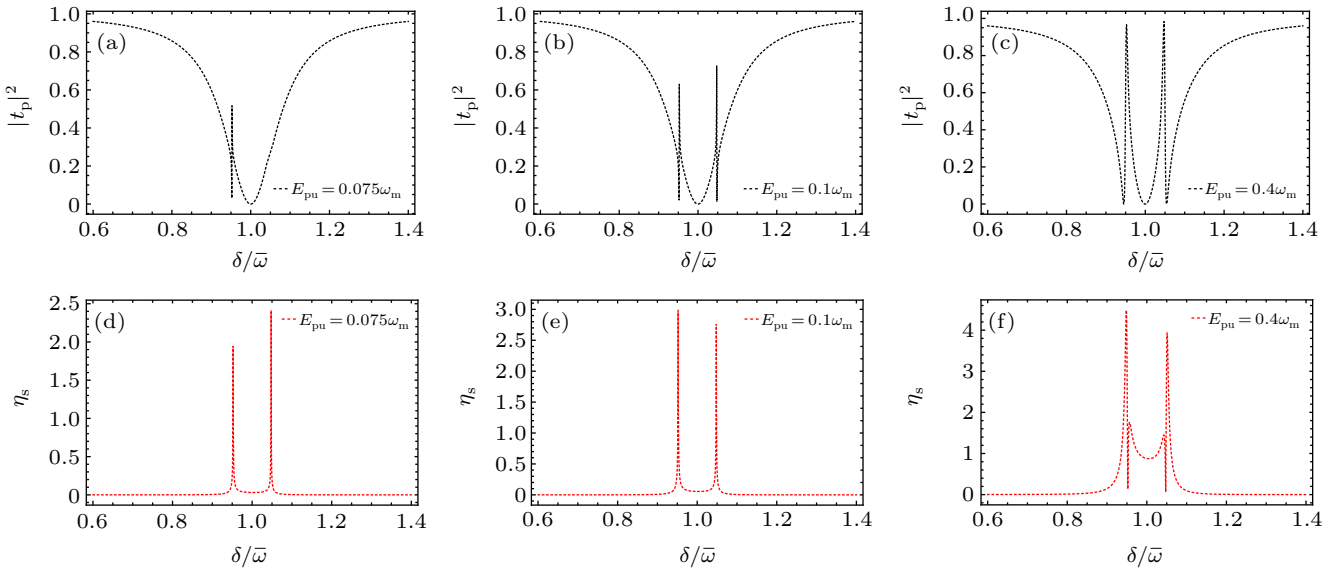


Fig. 3. Calculation results of the transmission intensity $|t_p|^2$ and the dimensionless amplitude of the second-order sideband η_s vary with $\delta/\bar{\omega}$ for different control field intensities: in panels (a) and (d), we use $E_{pu} = 0.075\omega_m$; in panels (b) and (e), we use $E_{pu} = 0.1\omega_m$; and in panels (c) and (f), we use $E_{pu} = 0.4\omega_m$. The other parameters are $g_0 = 2\pi \times 10.9$ MHz, $N = 2.3 \times 10^4$, $\Omega_c = 2\pi \times 15.2$ kHz, $\omega_m = 1.1\Omega_c$, $\Delta_a = 2\pi \times 32$ GHz, $\kappa = 2\pi \times 1.3$ kHz, and $\gamma_c = \gamma_m = 0.001\kappa$.

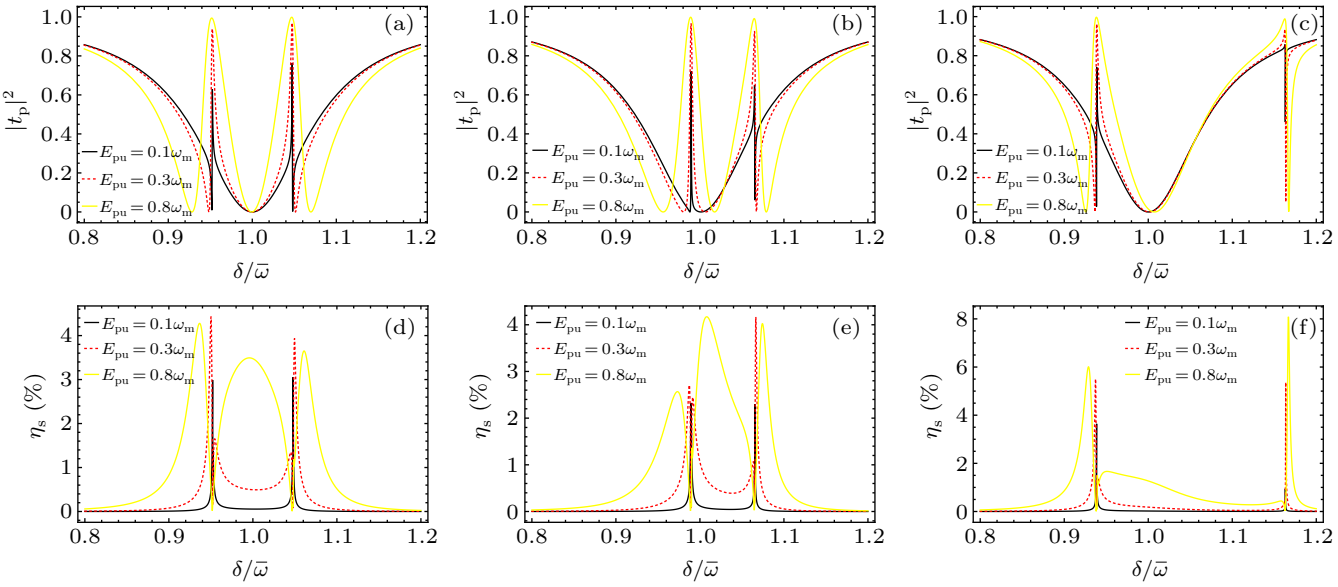


Fig. 4. Calculation results of the transmission intensity $|t_p|^2$ and the dimensionless amplitude of the second-order sideband η_s vary with $\delta/\bar{\omega}$ for different control field intensities: $E_{pu} = 0.1\omega_m$ (black line), $E_{pu} = 0.3\omega_m$ (red dash line), $E_{pu} = 0.8\omega_m$ (yellow line), meanwhile, calculated for different atom–atom interactions: in panels (a) and (d), we use $\omega_{sm} = 0$; in panels (b) and (e), we use $\omega_{sm} = 0.5\omega_r$; and in panels (c) and (f), we use $\omega_{sm} = \omega_r$. The other parameters are the same as those in Fig. 3.

Secondly, in order to observe the effect of atom–atom interaction on the transmission intensity $|t_p|^2$ and the dimensionless amplitude η_s of the SS, we have plotted $|t_p|^2$ and η_s of the system whether in the absence of BEC or in the presence of BEC in Fig. 4. There are three different interaction values: $\omega_{sm} = 0$ (Figs. 4(a) and 4(d)), $\omega_{sm} = 0.5\omega_r$ (Figs. 4(b) and 4(e)), and $\omega_{sm} = \omega_r$ (Figs. 4(c) and 4(f)). Meanwhile, we have plotted the transmission intensity $|t_p|^2$ and the efficiency amplitude η_s of the SS, versus the normalized cavity-pump detuning $\delta/\bar{\omega}$ for different control field intensities: $E_{pu} = 0.1\omega_m$ (black line), $E_{pu} = 0.3\omega_m$ (red dash line), $E_{pu} = 0.8\omega_m$ (yellow line).

In Figs. 4(a) and 4(d), without considering the atom–atom interaction strength $\omega_{sm} = 0$, so all three curves have two symmetrical OMIT windows, and the transparent window widens as the strength increases. For the comparison of the effect of the atom–atom interaction strength on the transmission intensity $|t_p|^2$ and the dimensionless amplitude η_s of the SS, considering interacting BEC with $\omega_{sm} = 0.5\omega_r$ (Figs. 4(b) and 4(e)) and $\omega_{sm} = \omega_r$ (Figs. 4(c) and 4(f)) respectively. Figures 4(b) and 4(e) show $|t_p|^2$ and η_s vary with $\delta/\bar{\omega}$ under a stronger atom–atom interaction $\omega_{sm} = 0.5\omega_r$, a very obvious phenomenon is that symmetrical OMIT windows become asymmetrical. Figures 4(c) and 4(f) show $|t_p|^2$ and η_s vary with $\delta/\bar{\omega}$ under much stronger atom–atom interaction $\omega_{sm} = \omega_r$, in addition to the symmetrical transparent window becoming asymmetrical, the position of the other OMIT window becomes farther away as increase the strength of the atom–atom interaction $\omega_{sm} = \omega_r$ (Figs. 4(c) and 4(f)). The reason can be explained as follow, based on the frequency of the Bogoliubov mode $\Omega_c = \sqrt{(4\omega_r + \frac{1}{2}\omega_{sm})(4\omega_r - \frac{1}{2}\omega_{sm})}$, we can see that Ω_c increases monotonically in terms of ω_{sm}. This means that as the ω_{sm} increases, the Bogoliubov mode Ω_c must change. The frequency difference between the Bogoliubov mode and the moving end mirror breaks the symmetry of the OMIT interference, and then the symmetric OMIT window becomes asymmetric. This is one of the advantages of a hybrid COMS over a bare system, where the frequency is a fixed-invariant parameter for a system consisting of the moving mirror. Due to the s-wave scattering frequency ω_{sm} can be controlled by Fechbach resonance, the hybrid COMS composed of Bogoliubov modes Ω_c can be controlled experimentally.

The effective frequency detuning is an important parameter for modulating the hybrid COMS. So we show the transmission intensity $|t_p|^2$ (see Figs. 5(a)–5(c)) and the dimensionless amplitude η_s of the SS (see Figs. 5(d)–5(f)) varying with probe–pump detuning $\delta/\bar{\omega}$ and the effective atom–pump detuning $\Delta/\bar{\omega}$ for three different atom–atom interaction values: $\omega_{sm} = 0.5\omega_r$ (Figs. 5(a) and 5(d)), $\omega_{sm} = \omega_r$ (Figs. 5(b) and 5(e)), and $\omega_{sm} = 1.5\omega_r$ (Figs. 5(c) and 5(f)). We can find that $|t_p|^2$ and η_s sensitively depend on the effective atom–pump detuning Δ. With the atom–atom interaction strength increasing, the local maximums of $|t_p|^2$ and η_s have greatly enhanced at the non-resonant position of the probe–pump detuning. In fact, the detuning regulation of nonlinear response plays a very important role in optical nonlinear modulation. The effective frequency detuning between the cavity field and the control field can change the transmission intensity and affect the dimensionless amplitude of the SS output. Comparison of $|t_p|^2$ in Figs. 5(a)–5(c) with η_s in Figs. 5(d)–5(f), the maximums of $|t_p|^2$ and η_s are always located in the very narrow frequency range for a fixed probe–pump detuning, and their corresponding transmission intensity $|t_p|^2$ and η_s present an asymmetric dip, as shown in Fig. 4.

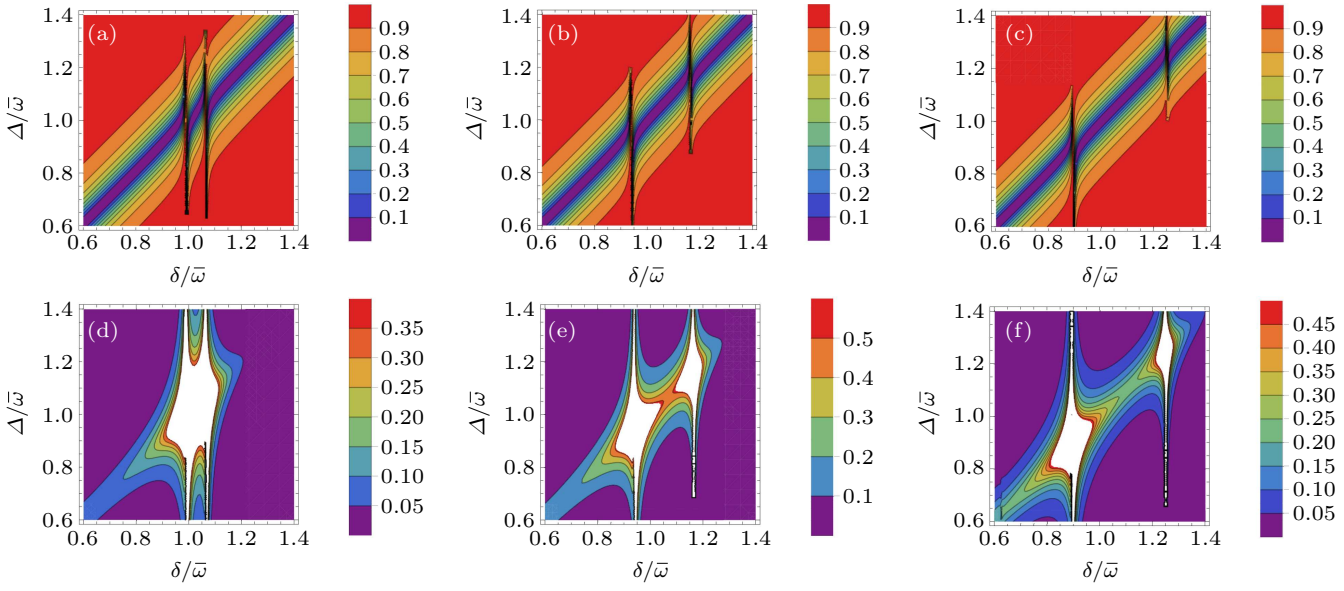


Fig. 5. Contour maps of the transmission intensity $|t_p|^2$ including [(a)–(c)] and the dimensionless amplitude of the second-order sideband η_s including [(d)–(f)] as a function of the effective atom–pump detuning $\Delta/\bar{\omega}$ and the control field detuning $\delta/\bar{\omega}$ with different atom–atom interaction strengths: $\omega_{sm} = 0.5\omega_r$ in panels (a) and (d), $\omega_{sm} = \omega_r$ in panels (b) and (e), and $\omega_{sm} = 1.5\omega_r$ in panels (c) and (f). The other parameters are the same as those in Fig. 3.

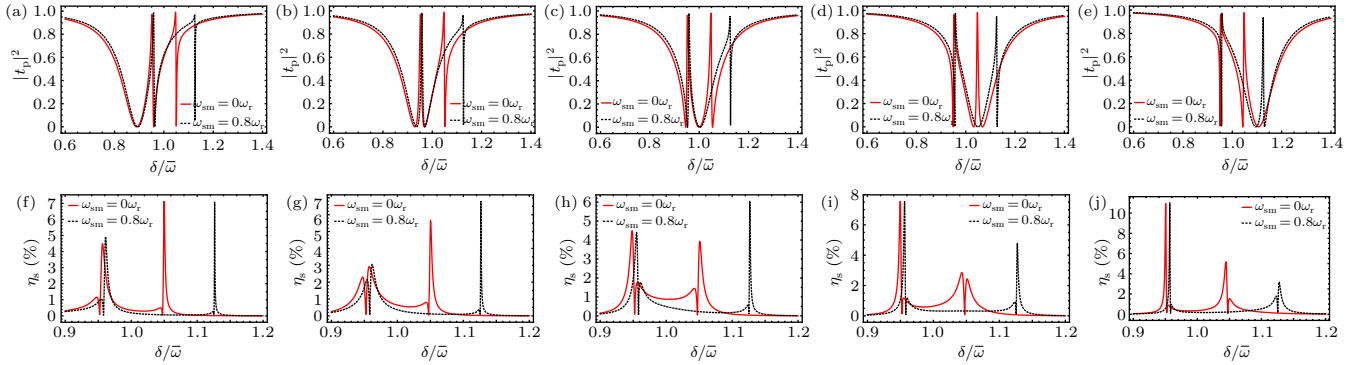


Fig. 6. Calculation results of the transmission intensity $|t_p|^2$ and the dimensionless amplitude of the second-order sideband η_s vary with $\delta/\bar{\omega}$ for different atom–pump detunings: $\Delta = 0.9\bar{\omega}$, $\Delta = 0.95\bar{\omega}$, $\Delta = \bar{\omega}$, $\Delta = 1.05\bar{\omega}$, and $\Delta = 1.1\bar{\omega}$. The red line for $\omega_{sm} = 0$ and the black dash line for $\omega_{sm} = 0.8\omega_r$. The other parameters are the same as those in Fig. 3.

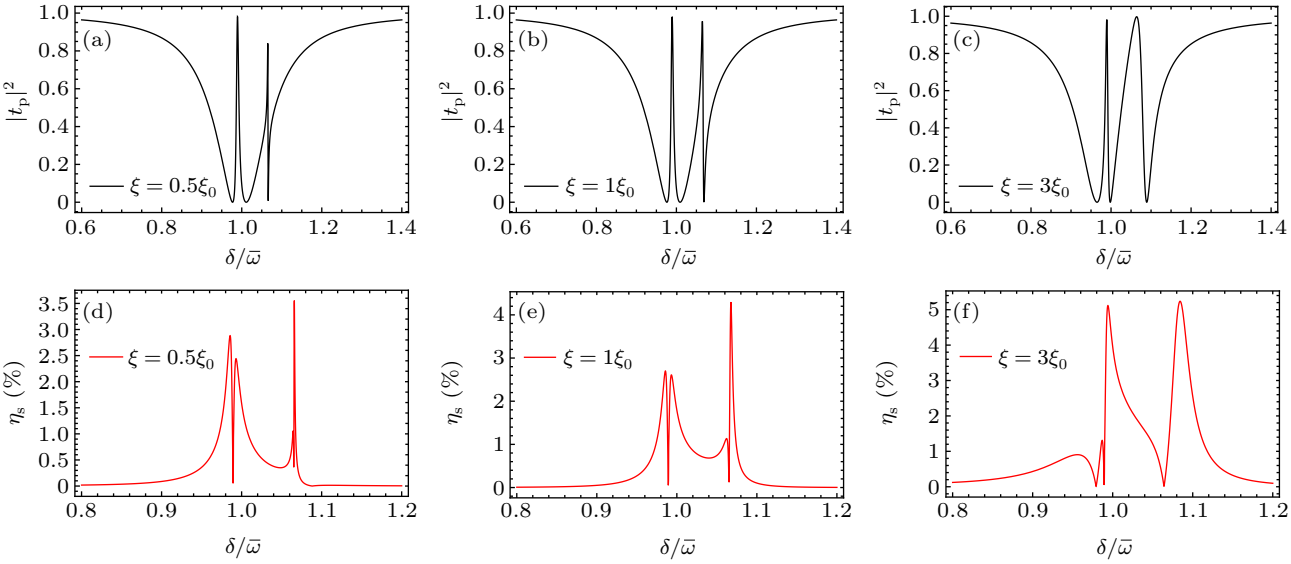


Fig. 7. Calculation results of the transmission intensity $|t_p|^2$ and the dimensionless amplitude of the second order sideband η_s vary with $\delta/\bar{\omega}$ for different effect coupling strengths: $\xi = 0.5\xi_0$, $\xi = \xi_0$, $\xi = 3\xi_0$. The other parameters are the same as those in Fig. 3.

The results also confirm that the effective frequency detuning of the control field is a very significant parameter, which enables us to change the transmission intensity $|t_p|^2$ and improve the dimensionless amplitude η_s of the SS. In order to see the effective atom–pump detuning Δ on the transmission intensity $|t_p|^2$ and the dimensionless amplitude η_s, we plot $|t_p|^2$ and η_s as a function of the probe–pump detuning $\delta/\bar{\omega}$ for different atom–pump detunings: $\Delta = 0.9\bar{\omega}$, $\Delta = 0.95\bar{\omega}$, $\Delta = \bar{\omega}$, $\Delta = 1.05\bar{\omega}$, and $\Delta = 1.1\bar{\omega}$ in Fig. 6. We can see clearly from the figure, the transmission intensity $|t_p|^2$ of the probe field and the dimensionless amplitude η_s of the SS generation can be modulated efficiently by adjusting the effective detuning Δ. Comparing $|t_p|^2$ in Figs. 6(a)–6(e) with η_s in Figs. 6(f)–6(j), when the effective atom–pump detuning $\Delta = \bar{\omega}$, the transmission intensity $|t_p|^2$ of the probe field and the dimensionless amplitude η_s of the SS generation presents symmetrical profile with two splitting peaks. However, when $\Delta = 0.9\bar{\omega}$, $\Delta = 0.95\bar{\omega}$ is tuned to less than $\bar{\omega}$, or when $\Delta = 1.05\bar{\omega}$, $\Delta = 1.1\bar{\omega}$ is tuned to more than $\bar{\omega}$ on the atom–atom interaction strength $\omega_{sm} = 0$, on the one hand, a very obvious phenomenon is that symmetrical transparency windows become asymmetrical; on the other hand, when $\Delta < \bar{\omega}$, the right peak of the effective amplitude η_s profile is enhanced remarkably which can see Figs. 6(f) and 6(g), while $\Delta > \bar{\omega}$, the left peak of the effective amplitude η_s profile is amplified significantly which can see Figs. 6(i) and 6(j). However, even the effective atom–pump detuning $\Delta = \bar{\omega}$, when the atom–atom interaction strength $\omega_{sm} = 0.8\omega_r$, comparing the red line with the black dash line in Figs. 6(c) and 6(h), there are two pronounced phenomena, one is that the symmetry of the profile is broken, another one is that the right peak is away from the center. In addition, when the effective atom–pump detuning $\Delta \neq \bar{\omega}$, the phenomenon is the same as that without the atom–atom interaction strength. It is well known that the exchange between phonons and photons can be effectively controlled by modulating efficient atom–pump detuning Δ. Thus, the density of the photons in the cavity and the photon pressure on the mechanical resonator can also be tuned to each other by effective atom–pump detuning Δ. So the transmission intensity $|t_p|^2$ and the dimensionless amplitude η_s of the SS generation will

be adjusted significantly.

Finally, the transmission intensity $|t_{\rm p}|^2$ and the dimensionless amplitude $\eta_{\rm s}$ are plotted as the probe–pump detuning $\delta/\bar{\omega}$ for the effect coupling strengths: $\xi = 0.5\xi_0$, $\xi = \xi_0$, $\xi = 3\xi_0$ in Fig. 7. With the increase of effect coupling ξ between Bogoliubov and optical mode, not only the SS effect can be produced, but also the left peak value increases significantly. The stronger of the effective coupling strength is, the higher of the peak will get. It can be seen that the stronger SS effect can achieve in such kind of a hybrid COMS. By controlling the coupling intensity between Bogoliubov and the optical mode, the generation efficiency of the SS can improve obvious.

4. Conclusion

In conclusion, we theoretically and numerically analyzed the nonlinear optical transmission characteristics of a hybrid COMS in which a BEC is trapped inside an optical cavity with a moving end mirror. First of all, we obtained the analytical expressions of the transmission intensity $|t_{\rm p}|^2$ and the dimensionless amplitude $\eta_{\rm s}$ of the SS. The tunable SS effects can be obtained by using the atom–atom two-body interaction as a new handle. It is one of the most exciting features of such hybrid COMS containing the BEC, we can obtain the controllability of the frequency of the Bogoliubov mode which can be altered by using the s-wave scattering interaction. Moreover, it has been shown that numerical results show that the transmission intensity $|t_{\rm p}|^2$ and the dimensionless amplitude $\eta_{\rm s}$ of the SS can be adjusted by the COMS parameters, including the control field intensities, the effective detuning, and the effective coupling strength.

To demonstrate that the transmission intensity $|t_{\rm p}|^2$ and the dimensionless amplitude $\eta_{\rm s}$ of the SS investigated here are within the experimental reach, we discussed the experimental parameters from Refs. [49,50], a BEC of typically $N = 2.3\times10^4$ ^{87}Rb atoms is coupled to the light field of an optical ultra-high finesse Fabry–Pérot cavity. The atom–field coupling $g_0 = 2\pi\times10.9$ MHz and typically atom–pump detuning is $\Delta_{\rm a} = 2\pi\times32$ GHz. We choose a particular set of parameters and procedures very close to the present experimental ventures, which makes our study experimentally feasible. We believe that this new method of generation of the SS proposed in this paper will implemente by the present experiments shortly.

Appendix A: Derivation of SS analytical expressions

Here we provide some details about the SS analytical expressions. We substitute Eqs. (16)–(20) into Eqs. (11)–(15), and compare the coefficients in the same order. After some calculations, we can obtain the first-order sideband equations as follows:

$$(\kappa+\mathrm{i}\Delta-\mathrm{i}\delta)c_1^- = -\mathrm{i}\xi c_0 X_1^- + \mathrm{i}Gc_0 q_1^- + E_{\rm pr}, \tag{A1}$$

$$(\kappa+\mathrm{i}\Delta+\mathrm{i}\delta)c_1^+ = -\mathrm{i}\xi c_0 X_1^+ + \mathrm{i}Gc_0 q_1^+, \tag{A2}$$

$$-\mathrm{i}\delta X_1^- = \Omega_{\rm c} Y_1^- - \gamma_{\rm c} X_1^-, \tag{A3}$$

$$\mathrm{i}\delta X_1^+ = \Omega_{\rm c} Y_1^+ - \gamma_{\rm c} X_1^+, \tag{A4}$$

$$-\mathrm{i}\delta Y_1^- = -\Omega_{\rm c} X_1^- - \gamma_{\rm c} Y_1^- - \xi[c_0^* c_1^- + c_0 c_1^{+*}], \tag{A5}$$

$$\mathrm{i}\delta Y_1^+ = -\Omega_{\rm c} X_1^+ - \gamma_{\rm c} Y_1^+ - \xi[c_0^* c_1^+ + c_0 c_1^{-*}], \tag{A6}$$

$$-\mathrm{i}\delta q_1^- = \omega_{\rm m} p_1^-, \tag{A7}$$

$$\mathrm{i}\delta q_1^+ = \omega_{\rm m} p_1^+, \tag{A8}$$

$$-\mathrm{i}\delta p_1^- = -\omega_{\rm m} q_1^- - \gamma_{\rm m} p_1^- + G[c_0^* c_1^- + c_0 c_1^{+*}], \tag{A9}$$

$$\mathrm{i}\delta p_1^+ = -\omega_{\rm m} q_1^+ - \gamma_{\rm m} p_1^+ + G[c_0^* c_1^+ + c_0 c_1^{-*}]. \tag{A10}$$

Based on the steady-state solutions Eqs. (8)–(10), we find the first-order sideband analytical expressions

$$c_1^- = \frac{(1+\mathrm{i}f_1(\delta)+\mathrm{i}f_2(\delta))E_{\rm pr}}{\kappa+\mathrm{i}\Delta-\mathrm{i}\delta-2\Delta f_1(\delta)-2\Delta f_2(\delta)}, \tag{A11}$$

$$X_1^- = \frac{-\lambda_1(\delta)\xi c_0^* E_{\rm pr}}{\kappa+\mathrm{i}\Delta-\mathrm{i}\delta-2\Delta f_1(\delta)-2\Delta f_2(\delta)}, \tag{A12}$$

$$q_1^- = \frac{-\lambda_2(\delta)Gc_0^* E_{\rm pr}}{\kappa+\mathrm{i}\Delta-\mathrm{i}\delta-2\Delta f_1(\delta)-2\Delta f_2(\delta)}, \tag{A13}$$

where

$$\lambda_1(\delta) = \frac{\Omega_{\rm c}}{\Omega_{\rm c}^2+(\gamma_{\rm c}-\mathrm{i}\delta)^2}, \tag{A14}$$

$$\lambda_2(\delta) = \frac{\omega_{\rm m}}{\omega_{\rm m}^2-\delta^2-\mathrm{i}\delta\gamma_{\rm m}}, \tag{A15}$$

$$f_1(\delta) = \frac{\xi^2|c_0|^2\lambda_1(\delta)}{\kappa-\mathrm{i}\Delta-\mathrm{i}\delta}, \tag{A16}$$

$$f_2(\delta) = \frac{G^2|c_0|^2\lambda_2(\delta)}{\kappa-\mathrm{i}\Delta-\mathrm{i}\delta}. \tag{A17}$$

Then, we can get the SS equations as

$$(\kappa+\mathrm{i}\Delta-2\mathrm{i}\delta)c_2^- = -\mathrm{i}\xi(c_0X_2^- + c_1^-X_1^-) + \mathrm{i}G(c_0q_2^- + c_1^-q_1^-), \tag{A18}$$

$$(\kappa+\mathrm{i}\Delta+2\mathrm{i}\delta)c_2^+ = -\mathrm{i}\xi(c_0X_2^+ + c_1^+X_1^+) + \mathrm{i}G(c_0q_2^+ + c_1^+q_1^+), \tag{A19}$$

$$-2\mathrm{i}\delta X_2^- = \Omega_{\rm c}Y_2^- - \gamma_{\rm c}X_2^-, \tag{A20}$$

$$2\mathrm{i}\delta X_2^+ = \Omega_{\rm c}Y_2^+ - \gamma_{\rm c}X_2^+, \tag{A21}$$

$$-2\mathrm{i}\delta Y_2^- = -\Omega_{\rm c}X_2^- - \gamma_{\rm c}Y_2^- - \xi[c_0^*c_2^- + c_0c_2^{+*} + c_1^-c_1^{+*}], \tag{A22}$$

$$2\mathrm{i}\delta Y_2^+ = -\Omega_{\rm c}X_2^+ - \gamma_{\rm c}Y_2^+ - \xi[c_0^*c_2^+ + c_0c_2^{-*} + c_1^+c_1^{-*}], \tag{A23}$$

$$-2\mathrm{i}\delta q_2^- = \omega_m p_2^-, \tag{A24}$$

$$2\mathrm{i}\delta q_2^+ = \omega_{\rm m} p_2^+, \tag{A25}$$

$$-2\mathrm{i}\delta p_2^- = -\omega_\mathrm{m} q_2^- - \gamma_\mathrm{m} p_2^- + G[c_0^* c_2^- + c_0 c_2^{+*} + c_1^- c_1^{+*}], \tag{A26}$$

$$2\mathrm{i}\delta p_2^+ = -\omega_\mathrm{m} q_2^+ - \gamma_\mathrm{m} p_2^+ + G[c_0^* c_2^+ + c_0 c_2^{-*} + c_1^+ c_1^{-*}]. \tag{A27}$$

We find the SS analytical expressions and obtain c_2^- as follows:

$$c_2^- = \frac{-(\mathrm{i}f_1(2\delta)+\mathrm{i}f_2(2\delta))c_0(\xi X_1^- - G q_1^-)^2}{\kappa+\mathrm{i}\Delta-2\mathrm{i}\delta-2\Delta(f_1(2\delta)+f_2(2\delta))(\kappa-\mathrm{i}\Delta-\mathrm{i}\delta)} + \frac{(\delta(f_1(2\delta)+f_2(2\delta))-1)(\mathrm{i}\xi c_1^- X_1^- - \mathrm{i}G c_1^- q_1^-)}{\kappa+\mathrm{i}\Delta-2\mathrm{i}\delta-2\Delta(f_1(2\delta)+f_2(2\delta))(\kappa-\mathrm{i}\Delta-\mathrm{i}\delta)}, \tag{A28}$$

where

$$\lambda_1(2\delta) = \frac{\Omega_\mathrm{c}}{\Omega_\mathrm{c}^2+(\gamma_\mathrm{c}-2\mathrm{i}\delta)^2}, \tag{A29}$$

$$\lambda_2(2\delta) = \frac{\omega_\mathrm{m}}{\omega_\mathrm{m}^2-4\delta^2-2\mathrm{i}\delta\gamma_\mathrm{m}}, \tag{A30}$$

$$f_1(2\delta) = \frac{\xi^2|c_0|^2\lambda_1(2\delta)}{(\kappa-\mathrm{i}\Delta-2\mathrm{i}\delta)(\kappa-\mathrm{i}\Delta-\mathrm{i}\delta)}, \tag{A31}$$

$$f_2(2\delta) = \frac{G^2|c_0|^2\lambda_2(2\delta)}{(\kappa-\mathrm{i}\Delta-2\mathrm{i}\delta)(\kappa-\mathrm{i}\Delta-\mathrm{i}\delta)}. \tag{A32}$$

Acknowledgments

Project supported by the National Natural Science Foundation of China (Grant Nos. 11564034 and 21663026), the Natural Science Foundation of Gansu Province, China (Grant No. 20JR5RA509), the Fundamental Research Funds for the Central Universities of College of Electrical Engineering, Northwest Minzu University (Grant Nos. 31920210016, 31920190006, and 31920200006), and the Scientific Research Project of Hunan Educational Department, China (Grant No. 19B206).

References

[1] Kippenberg T J and Vahala K J 2008 *Science* **321** 1172
[2] Aspelmeyer M, Meystre P and Schwab K 2012 *Phys. Today* **65** 29
[3] Aspelmeyer M, Kippenberg T J and Marquardt F 2014 *Rev. Mod. Phys.* **86** 1391
[4] Mücke M, Figueroa E, Bochmann J, Hahn C, Murr K, Ritter S, Villas-Boas C J and Rempe G 2010 *Nature* **465** 755
[5] Agarwal G S and Huang S 2010 *Phys. Rev. A* **81** 041803
[6] Weis S, Rivière R, Deléglise S, Gavartin E, Arcizet O, Schliesser A and Kippenberg T J 2010 *Science* **330** 1520
[7] Zhang W, Qin L G, Tian L J and Wang Z Y 2021 *Chin. Phys. B* **30** 094203
[8] Safavi-Naeini A H, Mayer Alegre T P, Chan J, Eichenfield M, Winger M, Lin Q, Hill J T, Chang D and Painter O 2011 *Nature* **472** 69
[9] Liao Q H, Wang X Q, He G Q and Zhou L T 2021 *Chin. Phys. B* **30** 094205
[10] Kanamoto R and Meystre P 2010 *Phys. Rev. Lett.* **104** 063601
[11] Purdy T P, Brooks D W C, Botter T, Brahms N, Ma Z Y and Stamper-Kurn D M 2010 *Phys. Rev. Lett.* **105** 133602
[12] Xiong W, Jin D Y, Qiu Y Y, Lam C and You J Q 2016 *Phys. Rev. A* **93** 023844
[13] Dalafi A and Naderi M H 2017 *Phys. Rev. A* **95** 043601
[14] Xiong H, Si L G, Zheng A S, Yang X and Wu Y 2012 *Phys. Rev. A* **86** 013815
[15] Xiong H, Si L G, Yang X X and Wu Y 2015 *Appl. Phys. Lett.* **107** 091116
[16] Xiong H, Si L G, Lü X Y and Wu Y 2016 *Opt. Express* **24** 5773
[17] Li J, Yu R, Ma J and Wu Y 2015 *Phys. Rev. A* **91** 063834
[18] Jiao Y, Lu H, Qian J, Li Y and Jing H 2016 *New J. Phys.* **18** 083034
[19] Liu Z X, Xiong H and Wu Y 2018 *Phys. Rev. A* **97** 013801
[20] DelHaye P, Schliesser A, Arcizet O, Wilken T, Holzwarth R and Kippenberg T J 2007 *Nature* **450** 1214
[21] Li J, Yu R, Ding C, Wang W and Wu Y 2014 *Phys. Rev. A* **90** 033830
[22] Cao C, Chen X, Duan Y W, Fan L, Zhang R, Wang T J and Wang C 2017 *Optik* **130** 659
[23] Xu W L, Gao Y P, Cao C, Wang T J and Wang C 2020 *Phys. Rev. A* **102** 043519
[24] Lü X Y, Jing H, Ma J Y and Wu Y 2015 *Phys. Rev. Lett.* **114** 253601
[25] Urrios D N, Capuj N E, Colombano M F, García P D, Sledzinska M, Alzina F, Griol A, Martínez A and Sotomayor-Torres C M 2007 *Nature* **450** 1214
[26] Gao Y P, Cao C, Duan Y W, Liu X F, Pang T T, Wang T J and Wang C 2019 *Nanophotonics* **9** 1953
[27] Wang G L, Huang L, Lai Y C and Grebogi C 2014 *Phys. Rev. Lett.* **112** 110406
[28] Yang X H, Yin Z Y and Xiao M 2019 *Phys. Rev. A* **99** 013811
[29] Li Y and Zhu K 2013 *Photon. Res.* **1** 16
[30] Xiong H, Liu Z X and Wu Y 2017 *Opt. Lett.* **42** 3630
[31] Kong C, Xiong H and Wu Y 2017 *Phys. Rev. A* **95** 033820
[32] Li L, Yang W X, Zhang Y, Shui T, Chen A X and Jiang Z M 2018 *Phys. Rev. A* **98** 6800411
[33] Gao Y, Wang T J, Cao C, Mi S C, Yang D Q, Zhang Y and Wang C 2018 *IEEE Photon. J.* **9** 6800411
[34] Børkje K, Nunnenkamp A, Teufel J D and Girvin S M 2013 *Phys. Rev. Lett.* **111** 053603
[35] Liu X F, Li Y and Jing H 2016 *Sci. Rep.* **6** 27102
[36] Liu S, Yang W X, Zhu Z, Shui T and Li L 2018 *Opt. Lett.* **43** 9
[37] Li J H, Zhang S Z, Yu R, Zhang D and Wu Y 2014 *Phys. Rev. A* **90** 053832
[38] Cao C, Mi S C, Gao Y P, He L Y, Yang D Q, Wang T J, Zhang R and Wang C 2016 *Sci. Rep.* **6** 22920
[39] Cao C, Mi S C, Wang T J, Zhang R and Wang C 2016 *IEEE J. Quantum Electron.* **52** 2563779
[40] Paternostro M, Kim M S and Ham B S 2003 *Phys. Rev. A* **67** 023811
[41] Agarwal G S and Huang S 2010 *Phys. Rev. A* **81** 041803
[42] Huang S 2014 *J. Phys. B: At. Mol. Opt. Phys.* **47** 055504
[43] Seok H, Buchmann L F, Singh S and Meystre P 2012 *Phys. Rev. A* **86** 063829
[44] Qu K and Agarwal G S 2013 *Phys. Rev. A* **87** 063813
[45] Wang H, Gu X, Liu Y X, Miranowicz A and Nori F 2014 *Phys. Rev. A* **90** 023817
[46] Akram M J, Ghafoor F and Saif F 2015 *J. Phys. B: At. Mol. Opt. Phys.* **48** 065502
[47] Bemani F, Motazedifard A, Roknizadeh R, Naderi M H and Vitali D 2017 *Phys. Rev. A* **96** 023805
[48] Gupta S, Moore K L, Murch K W and Stamper-Kurn D M 2007 *Phys. Rev. Lett.* **99** 213601
[49] Brennecke F, Donner T, Ritter S, Bourdel T, Kohl M and Esslinger T 2008 *Nature* **450** 268
[50] Brennecke F, Ritter S, Donner T and Esslinger T 2008 *Science* **322** 235
[51] Bhattacherjee A B 2009 *Phys. Rev. A* **80** 043607
[52] Bhattacherjee A B 2010 *J. Phys. B: At. Mol. Opt. Phys.* **43** 205301
[53] Kanamoto R and Meystre P 2010 *Phys. Scr.* **82** 038111
[54] Asjad M and Saif F 2011 *Phys. Rev. A* **84** 033606
[55] Chiara G D, Paternostro M and Palma G M 2011 *Phys. Rev. A* **83** 052324
[56] Rogers B, Paternostro M, Palma G M and Chiara G D 2012 *Phys. Rev. A* **86** 042323
[57] Dalafi A and Naderi M H 2017 *Phys. Rev. A* **96** 033631
[58] Mahajan S, Kumar T, Bhattacherjee A B and Mohan M 2013 *Phys. Rev. A* **87** 013621
[59] Mahajan S, Aggarwal N, Bhattacherjee A B and Mohan M 2013 *J. Phys. B: At. Mol. Opt. Phys.* **46** 085301
[60] Dalafi A, Naderi M H, Soltanolkotabi M and Barzanjeh S 2013 *J. Phys. B: At. Mol. Opt. Phys.* **46** 235502

[61] Yasir K A, Zhuang L and Liu W M 2017 *Phys. Rev. A* **95** 013810
[62] Motazedifard A, Bemani F, Naderi M H, Roknizadeh R and Vitali D 2016 *New J. Phys.* **18** 073040
[63] Molignini P, Papariello L, Lode A U J and Chitra R 2018 *Phys. Rev. A* **98** 053620
[64] Yasir K A and Liu W M 2016 *Sci. Rep.* **6** 22651
[65] Javed Akram M, Ghafoor F, Miskeen Khan M and Saif F 2017 *Phys. Rev. A* **95** 023810
[66] Liu L W, Gengzang D J, An X J and Wang P Y 2018 *Chin. Phys. B* **27** 034205
[67] Liu L W, Zhang G H, An X J, Hai L, Jiao H Y and Wang P Y 2019 *Laser Phys.* **29** 065501
[68] Zhang K, Chen W, Bhattacharya M and Meystre P 2010 *Phys. Rev. A* **81** 013802
[69] Nagy D, Szirmai G and Domokos P 2013 *Eur. Phys. J. D* **67** 124
[70] Morsch O and Oberthaler M 2006 *Rev. Mod. Phys.* **78** 179